X, *Y*, and *Z* waves: Extended structures in nonlinear lattices

P. G. Kevrekidis,[1] J. Gagnon,[1] D. J. Frantzeskakis,[2] and B. A. Malomed[3]
[1]*Department of Mathematics and Statistics, University of Massachusetts, Amherst, Massachusetts 01003-4515, USA*
[2]*Department of Physics, University of Athens, Panepistimiopolis, Zografos, Athens 15784, Greece*
[3]*Department of Interdisciplinary Studies, Faculty of Engineering, Tel Aviv University, Tel Aviv 69978, Israel*
(Received 14 March 2006; published 17 January 2007)

We propose a new type of waveforms in two-dimensional (2D) and three-dimensional (3D) discrete media-multilegged extended nonlinear structures (ENSs), built as arrays of lattice solitons (tiles and stones, in the 2D and 3D cases, respectively). We study the stability of the tiles and stones analytically, and then extend them numerically to complete ENS forms for both 2D and 3D lattices, aiming to single out stable ENSs. The predicted patterns can be realized in Bose-Einstein condensates trapped in deep optical lattices, crystals built of microresonators, and 2D photonic crystals. In the latter case, the patterns provide for a technique for writing reconfigurable virtual partitions in multipurpose photonic devices.

DOI: 10.1103/PhysRevE.75.016607 PACS number(s): 05.45.Yv, 03.75.Lm

Introduction and setup. Studies of dynamics in discrete media and their continuum periodically modulated counterparts demonstrate very rapid progress in diverse contexts [1], such as optics of waveguide arrays and photorefractive crystals [2], Bose-Einstein condensates (BECs) in optical lattices [3], the denaturation of the DNA double-strand [4], and others. These efforts have resulted in the prediction and *creation* of a variety of novel nonlinear structures, such as discrete dipole [5], quadrupole [6], necklace [7], and other multipulse or multipole localized patterns [8,9], discrete vortices [10], ring solitons [11], and others [12].

Experiments aimed at the creation of discrete-soliton states are actually performed in continuum media, with strong material [2] or virtual (photonic) [2–12] lattices built into them. It has been demonstrated by comparison of the experimental results with numerical simulations of the discrete models, and also by dint of analysis based on the Wannier-function expansion of continuous models with strong lattices [13], that, in all physically relevant cases, the abovementioned experimental settings are well approximated by the appropriate discrete models.

The present work is motivated by the abovementioned achievements and recent developments in studies of *X* waves, which are quasilinear extended structures generated in three [14] and two [15] dimensions (3D and 2D), and even in quasidiscrete [16] media. *X* waves arise when the second-order differential operator in the corresponding wave equation is (effectively [17]) sign indefinite (a D'Alembertian instead of the Laplacian).

In this paper, we are dealing with the sign-definite discrete Laplacian (the sign indefiniteness in the discrete case can be introduced by the well-known staggering transformation [1], applied along one coordinate only). Instead of emulating continuous wave equations supporting *X* waves in the lattice medium, our aim is to construct stable extended nonlinear structures (ENSs) in discrete media. By their nature, ENSs are partly delocalized, ranging from a few to infinitely many sites. An essential difference between the quasilinear *X* waves in continua and the lattice ENSs reported below is that the latter are strongly nonlinear structures, built as arrays of individual lattice solitons ("tiles"); in that sense, they somewhat resemble weakly localized hypersolitons [18] and supervortices [8], constructed as finite ensembles of individual solitons. We initialize our considerations in a purely nonlinear [anticontinuum (AC)] limit, at zero value of lattice's linear intersite coupling, $\epsilon=0$, and then extend the analysis up to a finite value of ϵ at which the respective structure becomes unstable (we report patterns that are *continuable*, starting from the AC limit; of course, at $\epsilon=0$, one may construct arbitrary states that will not continue to $\epsilon>0$). Our analysis presents a variety of thus found stable ENS species, including *X*, *Y*, and *Z* waves and some others, each being stable in a finite interval of values of ϵ. These patterns may definitely be of interest to applications in both nonlinear-optical and matter-wave contexts (as discussed at the end of this paper). Especially promising may be a possibility to use the ENSs for the creation of reconfigurable virtual partitions in photonic-crystal (PC) and PC-fiber multiservers. We also note that, while stable 1D patterns in 2D continuous nonlinear models (and their interactions with 2D objects) were considered before [19], this work presents the first examples of stable 1D strings in 3D media.

We consider the ubiquitous discrete nonlinear Schrödinger (DNLS) equation

$$i\dot{u}_{\mathbf{n}} = -\epsilon(\Delta_2 u)_{\mathbf{n}} - |u_{\mathbf{n}}|^2 u_{\mathbf{n}}, \tag{1}$$

where $u_{\mathbf{n}}$ is a complex amplitude of the electromagnetic wave in an optical waveguide array (in the 2D case) [2,20], or the BEC wave function at nodes of a 2D or 3D optical lattice [21,13], $\mathbf{n}$ being the vectorial lattice index, Δ_2 the standard discrete Laplacian, and $\dot{u}_{\mathbf{n}}$ the derivative with respect to the evolution variable, i.e., the transmission distance in optical arrays, or t in the BEC model (or in a crystal built of microresonators [22]).

The analysis will start with presenting basic types of "tiles" of which the ENSs are to be initially composed in the AC limit $\epsilon=0$. Then, we will numerically extend these compositions into full ENS solutions for $\epsilon>0$, and select stable ones among them, in the 2D and 3D cases.

Analytical results. We look for solutions to Eq. (1) as $u_{\mathbf{n}}=\exp(i\Lambda t)\phi_{\mathbf{n}}$, with $\phi_{\mathbf{n}}$ obeying $f(\phi_{\mathbf{n}},\epsilon)\equiv\Lambda\phi_{\mathbf{n}}-\epsilon\Delta_2\phi_{\mathbf{n}}$

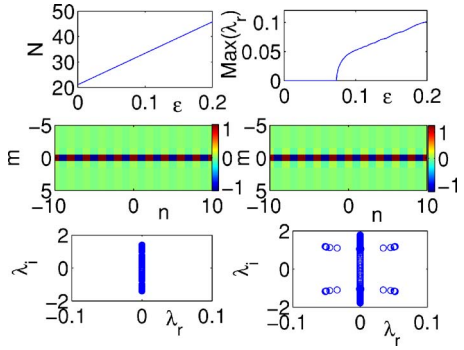

FIG. 1. (Color online) A family of single-leg patterns in the 2D model (configuration 1). The top left and right panels show, respectively, the norm and the largest instability growth rate vs ϵ. The contour plots in the middle panels display the stationary solutions for $\epsilon=0.05$ (stable) and $\epsilon=0.1$ (unstable). The spectral planes (λ_r, λ_i) of the eigenvalues for these solutions are presented in the bottom panels.

$-|\phi_{\mathbf{n}}|^2\phi_{\mathbf{n}}=0$. Perturbation of Eq. (1) around these solutions leads to the linearization operator

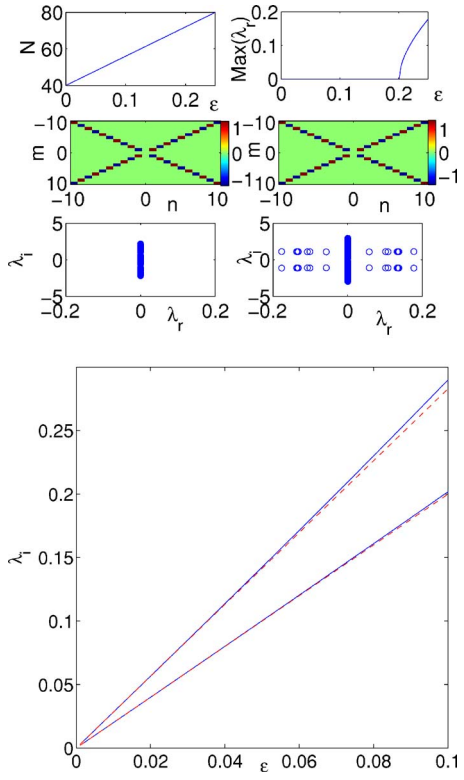

FIG. 2. (Color online) Same as in Fig. 1 but for configurations 2a (top three panels). The bottom panel presents the numerically obtained linear stability eigenvalues of tiles paving these patterns versus the analytical prediction (solid and dashed lines, respectively). The configurations are shown in the second row for $\epsilon=0.15$ (left) and 0.25 (right), and their corresponding stability is shown in the third row.

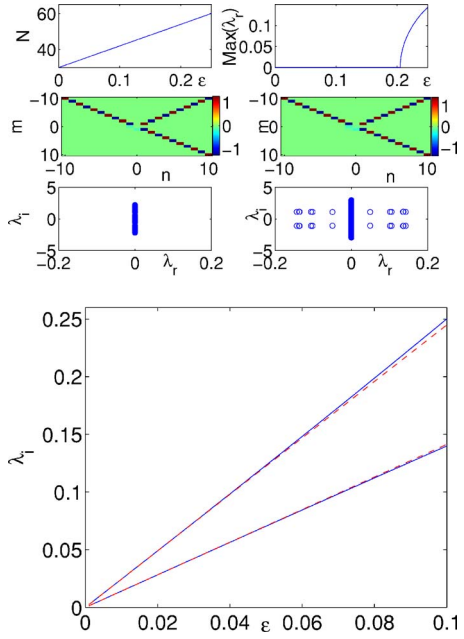

FIG. 3. (Color online) Identical as the previous figure, but for the configuration 2b.

$$\mathcal{H}_{\mathbf{n}}^{(\epsilon)}=\begin{pmatrix}\Lambda-2|\phi_{\mathbf{n}}|^2 & -\phi_{\mathbf{n}}^2\\ -(\phi_{\mathbf{n}}^*)^2 & \Lambda-2|\phi_{\mathbf{n}}|^2\end{pmatrix}-\epsilon\Delta_2\begin{pmatrix}1 & 0\\ 0 & 1\end{pmatrix}.$$

By rescaling, we fix $\Lambda\equiv 1$, while ϵ is kept as a free parameter.

For $\epsilon=0$, stationary solutions are $u_{\mathbf{n}}=re^{i\theta_{\mathbf{n}}}$, where real am-

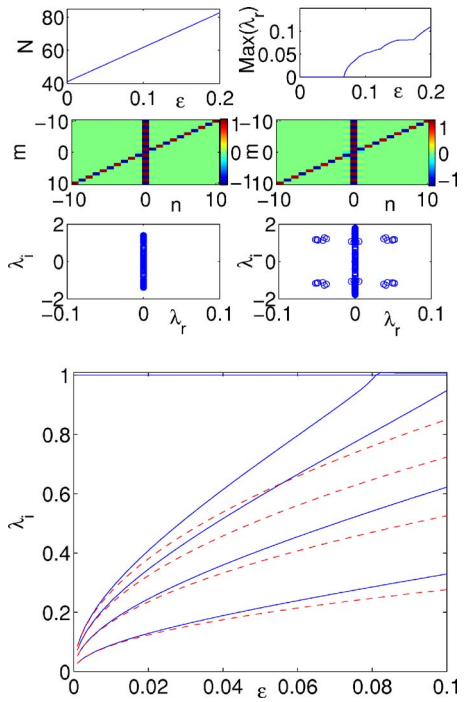

FIG. 4. (Color online) Same as the previous two figures, but for the configuration 2c. The second row panels show the solutions and the third row panels the stability for $\epsilon=0.05$ (left) and $\epsilon=0.2$ (right).

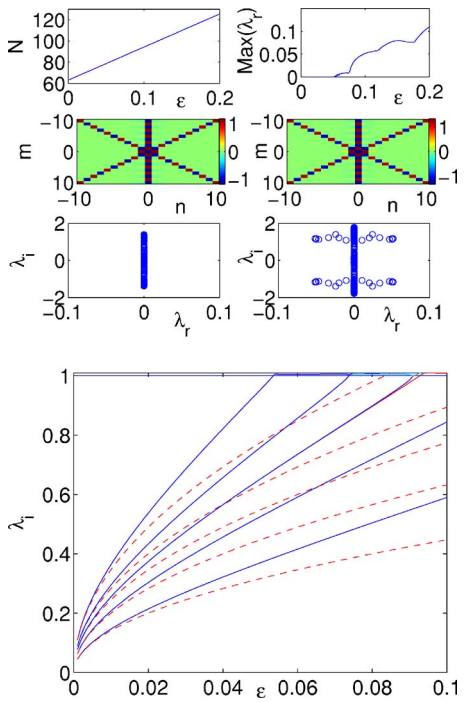

FIG. 5. (Color online) Same as the previous figures, but for configurations 3a. The second row panels show the solutions and the third row panels the stability for $\epsilon=0.05$ (left) and 0.1 (right).

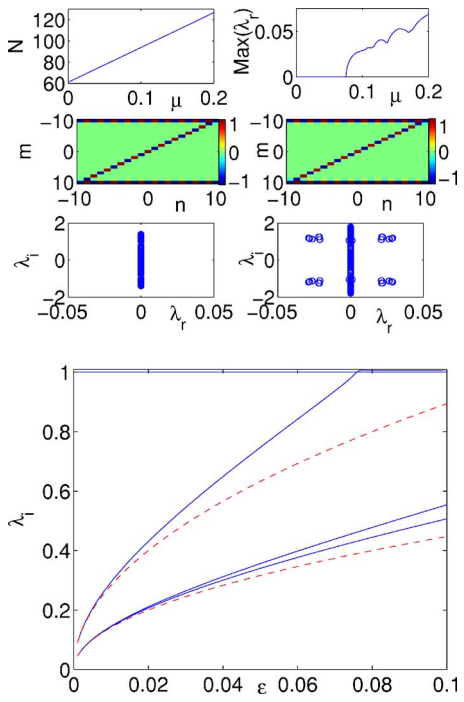

FIG. 6. (Color online) Identical to the previous figure, but for the configuration 3b.

plitude r is 0 or $\sqrt{\Lambda}$ and $\theta_{\mathbf{n}}$ are arbitrary phase constants. To continue the solutions to $\epsilon\neq 0$, a set of Lyapunov-Schmidt conditions need to be satisfied [23], viz., the projection of zero modes $\mathcal{H}^{(0)}_{\mathbf{n}}$ onto the system of stationary equations should be null, which leads to a solvability condition at each "AC-filled" site (one with $r\neq 0$ in the AC limit), $g_{\mathbf{n}}(\theta,\epsilon)\equiv(i\epsilon/2)[e^{-i\theta_{\mathbf{n}}}\Delta_2\phi_{\mathbf{n}}-e^{i\theta_{\mathbf{n}}}(\Delta_2\phi^*)_{\mathbf{n}}]=0$. Eigenvalues γ of the Jacobian, $\mathcal{M}_{ij}\equiv\partial g_i/\partial\theta_j$, are related, at leading order in ϵ, to eigenvalues (λ) of the linearization around the stationary solution by $\lambda=\pm\sqrt{2\gamma}$.We use this relation, alongside a perturbative expansion of the solution $\phi_{\mathbf{n}}=\phi^{(0)}_{\mathbf{n}}+\epsilon\phi^{(1)}_{\mathbf{n}}+\cdots$, to derive leading-order bifurcation conditions for ENSs and find the corresponding linear-stability eigenvalues for nonzero coupling.

ENSs in the 2D case can be categorized by the number of their "legs" (i.e., the number of quasi-1D strings of which it is composed). Simplest is the one-leg structure assembled of two- or three-site tiles, to which 1D stability results can be applied [23]. The respective Jacobian is

$$\mathcal{M}_{i,j}=\begin{cases}\cos(\theta_{j+1}-\theta_j)+\cos(\theta_{j-1}-\theta_j), & i=j,\\ -\cos(\theta_j-\theta_i), & i=j\pm 1,\\ 0, & |i-j|\geq 2,\end{cases}$$

from which conclusions for the stability of the one-leg ENSs may be drawn. In particular, a necessary (but not sufficient) stability condition is that the phase shift between adjacent sites must be π [23,24]. For the two-site tile satisfying this condition, the eigenvalues are imaginary (neutrally stable) [23], $\lambda=\sqrt{2\gamma}=\pm 2\sqrt{\epsilon}i$, while for its three-site counterpart, $(+1,-1,+1)$, they are $\lambda=\pm\sqrt{2\epsilon}i$ and $\lambda=\pm\sqrt{6\epsilon}i$. The (single-leg) chain assembled of these tiles is $(\ldots,-1,+1,-1,+1,-1,\ldots)$, is hereafter termed configuration 1.

Proceeding to two-tile configurations allows us to examine more complex (in particular, X and Y shaped) ENSs in 2D. The X configurations can be built of square- or cross-shaped tiles, which, at $\epsilon=0$, are

$$\begin{pmatrix}1&0&-1\\0&0&0\\-1&0&1\end{pmatrix}\quad\text{and}\quad\begin{pmatrix}1&0&1\\0&-1&0\\1&0&1\end{pmatrix}. \tag{2}$$

The latter one is not considered further, as it gives rise to an unstable eigenvalue pair, $\lambda=\pm 2\epsilon$ (despite the fact that this configuration meets the abovementioned necessary stability criterion, having the π phase shift between adjacent nonempty sites). The former tile has a pair of $\lambda=\pm 2\sqrt{2\epsilon}i$, and double $\lambda=\pm 2\epsilon i$, hence stable X configurations (to be called 2a) can be constructed at finite ϵ as arrays of such tiles with alternating signs.

Other two-leg configurations are Y shaped and "skew-X" ones, composed, respectively, of

$$\begin{pmatrix}1&0&-1\\0&0&0\\0&0&1\end{pmatrix}\quad\text{and}\quad\begin{pmatrix}0&-1&1\\0&1&0\\1&-1&0\end{pmatrix}. \tag{3}$$

Both these tiles are stable, with $\lambda=\pm\sqrt{2\epsilon}i$ and $\lambda=\pm\sqrt{6\epsilon}i$ for the former, and $\lambda=\pm 0.874\sqrt{\epsilon}i$, $\lambda=\pm 1.663\sqrt{\epsilon}i$, $\lambda=\pm 2.882\sqrt{\epsilon}i$, and $\lambda=\pm 2.690\sqrt{\epsilon}i$ for the latter. Stable sign-alternate ENSs assembled of them are termed 2b and 2c, respectively.

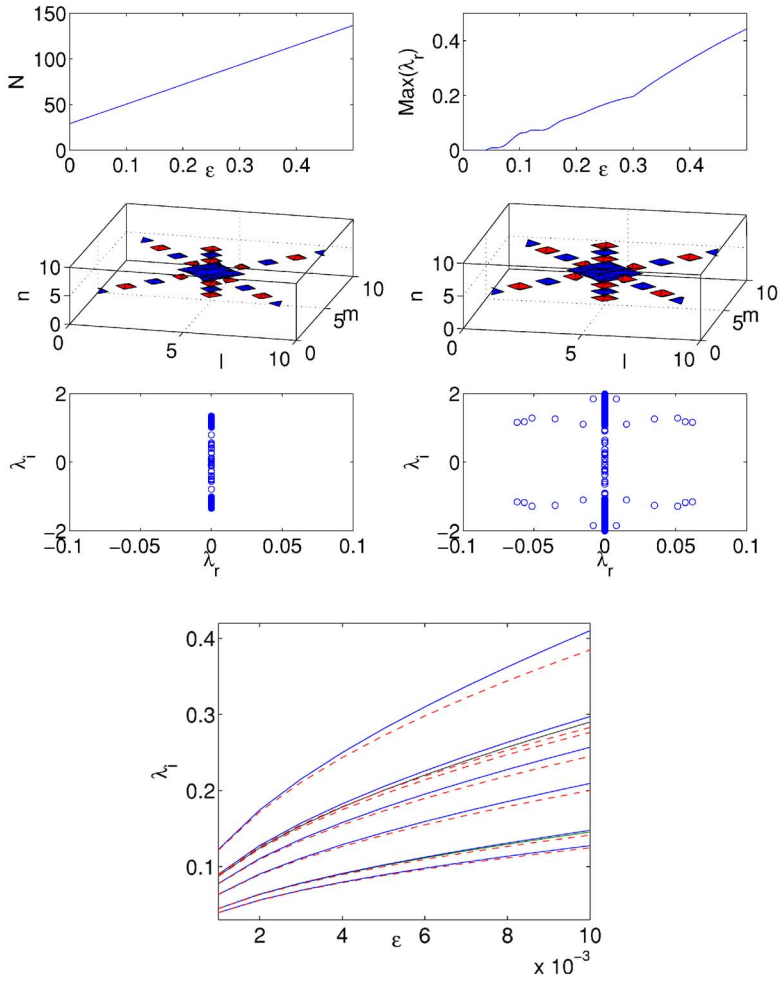

FIG. 7. (Color online) Same as above, but for 3D configuration 4a. The configurations and stability of the second and third row, respectively, are for $\epsilon=0.03$ (left) and $\epsilon=0.1$ (right).

The following tiles [generally, denser filled than their counterparts (3)] were shown by our analysis to be stable building blocks for three-leg ENSs,

$$\begin{pmatrix} 1 & -1 & 1 \\ -1 & 1 & -1 \\ 1 & -1 & 1 \end{pmatrix} \quad \text{and} \quad \begin{pmatrix} 1 & -1 & 1 \\ 0 & 1 & 0 \\ -1 & 0 & 0 \end{pmatrix}. \tag{4}$$

The former tile generates three pairs of double eigenvalues $\pm\sqrt{2\epsilon}i$, $\pm\sqrt{6\epsilon}i$, and $\pm\sqrt{8\epsilon}i$, and two pairs of single ones $\pm 2\sqrt{\epsilon}i$ and $\pm\sqrt{12\epsilon}i$. The latter tile has a double eigenvalue $\pm\sqrt{2\epsilon}i$ and a single one $\pm\sqrt{8\epsilon}i$. Three-leg ENSs paved by these tiles with alternating signs are called 3a and 3b, respectively. In fact, the latter one is a *Z*-shaped array.

Finally, we consider two configurations as a proof-of-principle of the extension of the ENS concept to the 3D space. In particular, augmenting the first tile of Eq. (4) by two −1 sites, adjacent to middle 1 along the third direction, we produce a "stone." The stone is stable, with single eigenvalues $\lambda=\pm 1.248\sqrt{\epsilon}i$, $\lambda=\pm 2\sqrt{\epsilon}i$, $\lambda=\pm\sqrt{6\epsilon}i$, $\lambda=\pm 2.763\sqrt{\epsilon}i$ and $\lambda=\pm 3.848\sqrt{\epsilon}i$, and double and triple ones, $\lambda=\pm\sqrt{8\epsilon}i$ and $\lambda=\pm\sqrt{2\epsilon}i$, respectively. The stones will be used to build a stable 3D pattern (again, with sign alternations), called 4a in our nomenclature.

The simplest stable stone is a "diamond" consisting of six AC-filled sites surrounding, as nearest neighbors, an empty one. Although configurations of this type (including ones satisfying the above necessary stability criterion of adjacently excited sites with π-phase difference) may be unstable [12], our method allows to identify a stable one. The latter carries a phase distribution that corresponds to a quadrupole in the plane, with phases $\pi/2$ or $3\pi/2$ lent to the two out-of-plane sites. This stone has triple and single eigenvalues, $\lambda=\pm 2\epsilon i$ and $\lambda=\pm 4\epsilon i$, respectively, and a higher-order one, at $\mathcal{O}(\epsilon^2)$, which is stable too. A stable 3D configuration, labeled 4b, is assembled of the "diamonds" with alternating signs.

Numerical results. In Figs. 1–8 we present, in a unified format, results of the numerical continuation of select stable (up to respective destabilization points) ENSs, starting from the AC limit. In Fig. 1, configuration 1 (a straight chain of sign-alternating tiles in 2D) is shown. Its norm $N=\Sigma_n|\phi_n|^2$ and maximum instability growth rate are shown, as a function of the intersite coupling, ϵ, in the top left and right panels. In the 21×21 lattice, the chain is unstable at $\epsilon\geq 0.074$ (we also repeated the reported computations with larger lattices up to 41×41; the critical values of ϵ change only by 0.001 or less). The middle and bottom panels display typical examples of stable and unstable configurations, and the spectral plane (λ_r,λ_i) of their numerically found (in)stability eigenvalues, $\lambda\equiv\lambda_r+i\lambda_i$, the instability being introduced by $\lambda_r\neq 0$. The results are reported herein for Dirichlet boundary conditions (BCs). The role of BCs is relatively

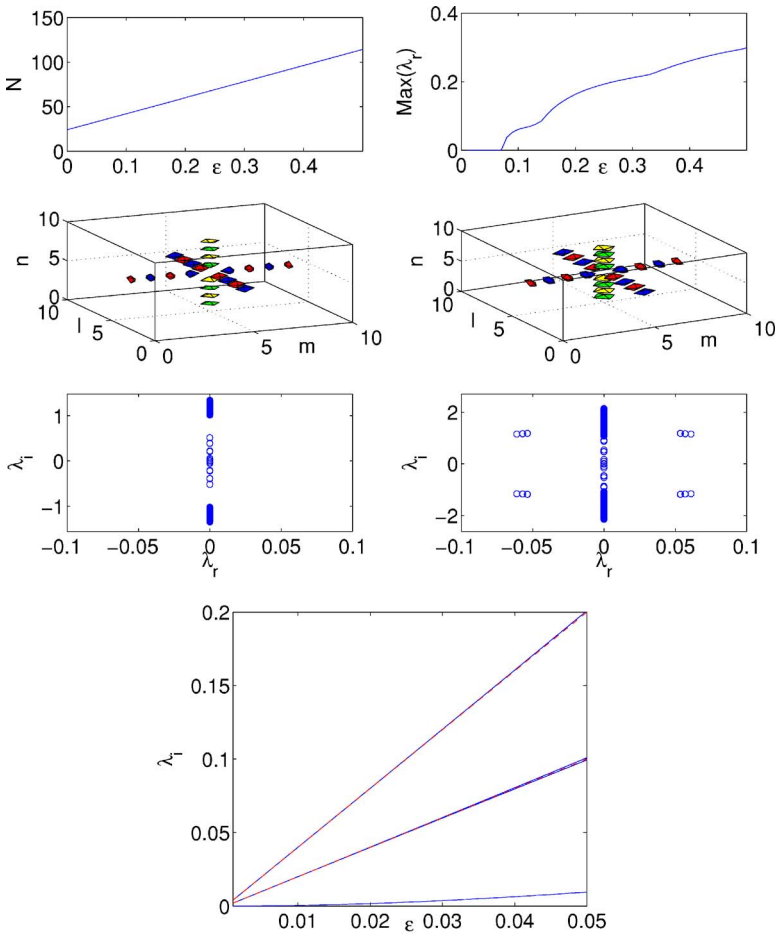

FIG. 8. (Color online) Same as in the previous figure but now for configuration 4b. In this case, the (green and yellow) out of plane sites have phase (in the limit of $\epsilon=0$) $\pi/2$ and $3\pi/2$, respectively.

weak (i.e., of higher order) in the Dirichlet and Neumann case. The periodic BC situation depends on the nature of the BC-imposed neighbors of the boundary sites (and their relative phase—see the discussion above).

Figures 2–4 present three different varieties of the two-leg configurations: 2a (X waves, Fig. 2), 2b (Y waves, Fig. 3) and 2c (skewed X waves, Fig. 4). Numerically computed stability eigenvalues of the corresponding tiles, i.e., the first one in Eq. (2) and both tiles in Eq. (3), are given by solid blue lines for comparison with the analytical predictions of the previous section (dashed red lines), showing good agreement. Configurations 2a, 2b, and 2c are unstable at $\epsilon \geq 0.202$, $\epsilon \geq 0.206$, and $\epsilon \geq 0.068$, respectively.

Similarly, Figs. 5 and 6 show two three-leg configurations, respectively, 3a and 3b and their stability. These configurations are found to be unstable at $\epsilon \geq 0.053$ and $\epsilon \geq 0.075$,
respectively, in our computations.

Finally, Figs. 7 and 8 show the continuation to $\epsilon \neq 0$ of 3D configurations 4a and 4b, which are stable, respectively, for $\epsilon \leq 0.043$ and $\epsilon \leq 0.075$. Note that the corresponding numerically computed eigenvalues (for the respective stones) again agree well with the analytical predictions.

Conclusion. We have presented a systematic approach towards constructing a variety of single- and multilegged extended nonlinear structures (ENSs) in 2D and 3D lattices. They are composed of building blocks, namely, tiles (2D) or stones (3D) with alternating signs, that are originally defined in the anticontinuum limit (the sign alternation is a necessary, but not sufficient, stability condition). Stable ENSs at small ϵ were selected analytically, and their stability intervals were revealed by numerical continuation in ϵ. Examination of nonlinear evolution of unstable patterns will be presented elsewhere.

One-legged ENSs have already been created in photorefractive crystals [9] through the launching of a stripe beam at various angles. Natural generalizations of these into the ENS patterns reported herein can be realized through the launch of sets of such beams. Furthermore, ENSs can be implemented in experiments with BECs trapped in deep optical lattices, photonic crystals (PCs) and/or PC fibers, and crystals composed of microresonators (MRs). In particular, the ENSs of a prescribed shape can be easily created by coupling a correspondingly patterned set of laser beams into the PC. In MR crystals, both 2D and 3D patterns can be created by exciting polaritons in the respective set of MRs, illuminating them with a laser source. In the BEC setting, a pattern can be written by optically removing the condensate from lattice sites that should be empty. Stable 2D ENSs can find applications as a technique for writing virtual partitions in PC-based integrated devices.

[1] S. Aubry, Physica D **103**, 201 (1997); S. Flach and C. R. Willis, Phys. Rep. **295**, 181 (1998); D. K. Campbell, S. Flach, and Y. S. Kivshar, Phys. Today **Jan**, 43 (2004).

[2] D. N. Christodoulides F. Lederer, and Y. Silberberg, Nature (London) **424**, 817 (2003); A. A. Sukhorukov, Y. S. Kivshar, H. S. Eisenberg, and Y. Silberberg,IEEE J. Quantum Electron. **39**, 31 (2003); J. W. Fleischer, G. Bartal, O. Cohen, T. Schwartz,O. Manela, B. Freedman, M. Segev, H. Buljan, and N. K. Efremidis, Opt. Express **13**, 1780 (2005).

[3] V. A. Brazhnyi and V. V. Konotop, Mod. Phys. Lett. B **18**, 627 (2004); P. G. Kevrekidis and D. J. Frantzeskakis, *ibid.* **18**, 173 (2004).

[4] M. Peyrard, Nonlinearity **17**, R1 (2004).

[5] J. Yang, I. Makasyuk, A. Bezryandina, and Z. Chen, Opt. Lett. **29**, 1662 (2004).

[6] J. Yang, I. Makasyuk, A. Bezryandina, and Z. Chen, Stud. Appl. Math. **113**, 389 (2004).

[7] J. Yang, I. Makasyuk, P. Kevrekidis, H. Martin, B. A. Malomed, D. J. Frantzeskakis, and Z. G. Chen, Phys. Rev. Lett. **94**, 113902 (2005).

[8] H. Sakaguchi and B. A. Malomed, Europhys. Lett. **72**, 698 (2005).

[9] Z. Chen, H. Martin, E. D. Eugenieva, J. J. Xu, and A. Bezryandina, Phys. Rev. Lett. **92**, 143902 (2004).

[10] D. N. Neshev, T. J. Alexander, E. A. Ostrovskaya, Y. S. Kivshar, H. Martin, I. Makasyuk, and Z. G. Chen, Phys. Rev. Lett. **92**, 123903 (2004); J. W. Fleischer, G. Bartal, O. Cohen, O. Manela, M. Segev, J. Hudock, and D. N. Christodoulides, *ibid.* **92**, 123904 (2004).

[11] X. Wang, Z. Chen, and P. G. Kevrekidis, Phys. Rev. Lett. **96**, 083904 (2006).

[12] R. Carretero-González, P. G. Kevrekidis, B. A. Malomed, and D. J. Frantzeskakis, Phys. Rev. Lett. **94**, 203901 (2005); T. J. Alexander, E. A. Ostrovskaya, A. A. Sukhorukov, and Y. S. Kivshar, Phys. Rev. A **72**, 043603 (2005).

[13] G. L. Alfimov, P. G. Kevrekidis, V. V. Konotop, and M. Salerno, Phys. Rev. E **66**, 046608 (2002).

[14] J. Y. Lu and J. F. Greenleaf, IEEE Trans. Ultrason. Ferroelectr. Freq. Control **39**, 19 (1992); P. Di Trapani, G. Valiulis, A. Piskarskas, O. Jedrkiewicz, J. Trull, C. Conti, and S. Trillo, Phys. Rev. Lett. **91**, 093904 (2003); C. Conti, S. Trillo, P. Di Trapani, G. Valiulis, A. Piskarskas, O. Jedrkiewicz, and J. Trull, *ibid.* **90**, 170406 (2003).

[15] D. N. Christodoulides, N. K. Efremidis, P. Di Trapani, and B. A. Malomed, Opt. Lett. **29**, 1446 (2004).

[16] S. Droulias, K. Hizanidis, J. Meier, and D. Christodoulides, Opt. Express **13**, 1827 (2005).

[17] C. Conti and S. Trillo, Phys. Rev. Lett. **92**, 120404 (2004).

[18] J. R. Salgueiro, H. Michinel, and M. I. Rodas-Verde, nlin.PS/0603011 (unpublished).

[19] Y. S. Kivshar, A. Nepomnyashchy, V. Tikhonenko, J. Christou, and B. Luther-Davies, Opt. Lett. **25**, 123 (2000); E. DelRe, S. Trillo, and A. J. Agranat, *ibid.* **25**, 560 (2000); H. E. Nistazakis, D. J. Frantzeskakis, and B. A. Malomed, Phys. Rev. E **64**, 026604 (2001).

[20] P. G. Kevrekidis, K. Ø. Rasmussen, and A. R. Bishop, Int. J. Mod. Phys. B **15**, 2833 (2001).

[21] A. Trombettoni and A. Smerzi, Phys. Rev. Lett. **86**, 2353 (2001).

[22] J. E. Heebner and R. W. Boyd, J. Mod. Opt. **49**, 2629 (2002); P. Chak *et al.*, Opt. Lett. **28**, 1966 (2003).

[23] D. E. Pelinovsky, P. G. Kevrekidis, and D. J. Frantzeskakis, Physica D **212**, 1 (2005); D. E. Pelinovsky, P. G. Kevrekidis, and D. J. Frantzeskakis, *ibid.* **212**, 20 (2005).

[24] T. Kapitula, P. G. Kevrekidis, and B. A. Malomed, Phys. Rev. E **63**, 036604 (2001).